Engineering Science and Technology, an International Journal 24 (2021) 655–664

HOSTED BY

Contents lists available at ScienceDirect

Engineering Science and Technology, an International Journal

journal homepage: www.elsevier.com/locate/jestch

# The experimental study of the entropy generation and energy performance of nano-fluid flow for automotive radiators

Beytullah Erdoğan [a,*], İbrahim Zengin [a], Serdar Mert [b], Adnan Topuz [a], Tahsin Engin [b]

[a] Zonguldak Bülent Ecevit University, Mechanical Engineering Department, Zonguldak 67100, Turkey
[b] Sakarya University, Mechanical Engineering Department, Sakarya 54055, Turkey

ARTICLE INFO

*Article history:*
Received 27 August 2020
Revised 20 October 2020
Accepted 24 October 2020
Available online 14 November 2020

*Keywords:*
Nanofluid
Entropy generation
Automobile radiator
Irreversibility

ABSTRACT

The present study focuses on the energy performance, entropy generation, and irreversibility of the use of nanofluid in an industrial Peugeot automobile radiator (size: 250 × 301 × 60.4 mm, channel number: 34 and hydraulic diameter: 1.923 mm) with a louvered fin type. 50:50 EG – water which is widely used in existing automobile radiators and a new generation of EG – water – Al2O3 (0.5%) nanofluid have been compared. In order to examine the effect of variable operating conditions on thermal performance for both fluid mixtures, experiments have been performed at variable air velocity (4–5 m/s), variable coolant flow rate (10–15 – 20 lt/min), and an inlet temperature of 95 °C (real automobile conditions). Thermo-hydraulics calculations such as entropy generation, irreversibility, effectiveness, NTU, heat transfer rate, pumping power have been obtained from experimental data. Among conducted experiments, with increasing coolant flow rate, entropy generation increases on the airside, while decreasing on the coolant side. When the entropy generation due to temperature and pressure difference is compared, entropy production due to pressure difference can be neglected. It has been evaluated that the use of nanofluid increases the heat transfer rate by 9.52%, reducing the irreversibility by about 68% at the 4 m/s air velocity and 10 lt/min coolant flow.


## 1. Introduction

In the past decades, nanofluids continue to maintain their place in the literature, due to their wide range of uses and their thermal properties superior to other fluids. Nanofluids have been created by adding nanoparticles with certain concentration rates into a base fluid. It is well known that the thermal conductivity of solid materials in terms of their molecular arrangement is higher than that of the base fluid. Therefore, solid particles increase the average thermal conductivity of the mixture. Therefore, the use of nanofluids in many fields such as automobile radiators [1–4], CPU cooling systems [5], and solar thermal systems [6] are being investigated.

The development of thermal systems generally focuses on 2 topics, including geometric design and fluid selection optimization. For example, considering the heat exchangers, the geometric design includes parameters such as optimum hydraulic diameter, duct length, optimum collector distance, while fluid parameters include thermal conductivity, viscosity, adhesion & cohesion effects, corrosion effects, and density for the fluid. The use of nanofluid in an automobile radiator makes it more convenient to design radiator sizes in more compact dimensions as it increases thermal performance. The compact design of car radiators performs less drag force and less fuel consumption. However, there are some factors that limit the use of nanofluids in such systems. Important factors such as increased pumping power due to increased viscosity, complex motion of the particles, nanoparticles collapsing in the base fluid over time, and stabilization should be considered. Water for automobile radiator coolant has long been preferred as the base fluid due to its high conductivity coefficient and low viscosity. However, it has been used by mixing with anti-freeze fluids to prevent icing in cold weather conditions. For example; These anti-freeze fluids such as EG (Ethylene glycol) and PG (Propylene glycol) prevent the interaction of the fluid molecule with the surface, that is, preventing icing on the surface by reducing adhesion forces. Therefore, most researchers have preferred to try by adding the nanoparticles into a water-antifreeze mixture instead of pure water to examine the effect of nanofluid in radiators [7–9]. Although propylene glycol (PG) is superior to EG with lower freezing point and less toxic property, EG is preferred more because it gives better results in terms of thermal performance [10].

Chaurasia et al. [11] studied on an automobile radiator with elliptical tubes of the mixture of pure water and nanoparticles

* Corresponding author.
*E-mail address:* beytullah.erdogan@beun.edu.tr (B. Erdoğan).
Peer review under responsibility of Karabuk University.

https://doi.org/10.1016/j.jestch.2020.10.007
2215-0986/

**Nomenclature**

| | |
|---|---|
| $W_c$ | core width of radiator, mm |
| $H_c$ | core height of radiator, mm |
| $D_c$ | core depth of radiator, mm |
| $A_{cs}$ | core surface area of radiator, mm |
| Q | heat transfer, W |
| $P_f$ | fan power, W |
| $P_p$ | pump power, W |
| $\varepsilon$ | effectiveness |
| P | pressure, Pa |
| T | temperature, K |
| $\eta_f$ | fan efficiency |
| $\eta_p$ | pump efficiency |
| $\dot{m}$ | mass flow rate, kg/s |
| $\dot{\forall}$ | volume flow rate, $m^3/s$ |
| V | velocity, m/s |
| C | heat capacity rate |
| $C^*$ | capacity ratio |
| $\rho$ | density, $kg/m^3$ |
| c | specific heat, J/kgK |
| R | gas constant, J/kgK |
| $\phi$ | volume fraction |
| $S_{gen}$ | entropy generation, W/K |
| I | irreversibility, W |

*Subscripts*

| | |
|---|---|
| nf | nanofluid |
| bf | base fluid |
| np | nanoparticle |
| a | air |
| i | inlet |
| e | exit |
| cs | core surface |

*Abbreviations*

| | |
|---|---|
| NTU | number of transfer unit |
| PI | performance index |
| EG | ethylene glycol |
| CFR | coolant flow rate |

without anti-freeze. They worked the 4 different Al2O3 concentration rates (0%–0.1%–0.15%–2%). For 0.2% concentration, it was evaluated that Al2O3-water nanofluid increases the heat transfer rate by 44.29%, while the effectiveness is a maximum of 40.3%. Among different inlet coolant temperatures, they evaluated that the effectiveness is highest between 60 and 65 °C.

Atmaca et al. [1] examined the thermal performance of automobile radiators by mixing 4 different types of nanoparticles [(i) pure TiO2, (ii) TiO2 – %0.1 Ag, (iii) TiO2 – %0.3 Ag, and (iv) TiO2 – %0.1 Cu] with 50–50% EG & water. While TiO2 doped with 0.3% Ag has shown the best thermal performance, TiO2 doped with 0.1% Cu has shown the lowest heat transfer rate. It was clear that TiO2 doped with Cu decreases the thermal conductivity performance of the nanofluid, while mixture doped with Ag has shown better thermal conductivity performance than pure TiO2.

Liang and Mudawar [12] conducted a comprehensive review of publications on nanofluids. Although there are some differences between the comments of the authors, they have stated that nanofluids increase the heat transfer due to the increase of the thermal boundary layer in the entrance region of the channel, but this increase effect on the downstream is not much. In numerical studies for nanofluids, it was emphasized that the thermal conductivity and viscosity behavior of single-phase approaches could not be determined and this behavior could be estimated more accurately with two-phase discrete models. The authors evaluated that nanofluids are a useful technique for heat transfer, but also create many important practical problems (clustering, sedimentation, clogging of flow passages, and erosion to the heating surface).

Huminic et al. [13] conducted a numerical study of the performance of hybrid nanofluids in laminar flow conditions in a flattened tube to improve the heat transfer rate of compact heat exchangers used in the automotive industry. While MWCNT + Fe3O4 – water and ND + Fe3O4 – water hybrid nanofluids have increased the heat transfer rate compared to base fluid (water), MWCNT + Fe3O4 – water hybrid nanofluid have produced less entropy compared to the other.

Cardenas et al. [9] examined the thermohydraulics performance of the automotive radiator installed in a wind tunnel. They compared the effect of Graphene and Silver nanoparticles added to 50–50% EG & water (base fluid) as coolant. Nanofluid mixture doped with Ag has shown an increasing trend thermal performance compared to base fluid, while mixture doped with Graphene has shown a decreasing trend.

Selvam et al. [8] preferred Graphene platelets with low interface thermal resistance structure and high thermal conductivity property in order to increase the convection heat transfer coefficient (CHTC) in automobile radiators. They added Graphene structured platelets with concentration ratios ranging between 0.1% and 0.5% into 70% EG-30% water mixture as base fluid. They found the maximum increase rate of overall heat transfer coefficient (OHTC) as 104% for varying concentrations under constant inlet temperature conditions of 35°. They evaluated that when the concentration rate increases from 0.1% to 0.5%, the pressure drop increases from 5.31 kPa to 7.36 kPa and emphasized that the increase in pressure in these concentrations is advantageous compared to other nanofluids.

Zhao et al. [14] investigated the Al2O3 – water mixture through a commercial software using the finite volume method for a symmetrical flat tube. They used the single-phase approach modeling method because of less computational time and simpler implementation and adapted it to the model with variable conditions of temperature, concentration ratio, and particle size for the thermal conductivity coefficient. They evaluated an increase in heat transfer development with increasing nanoparticle concentration rate and nanoparticle size. They also observed a decrease in total entropy generation with the increasing concentration amount, while increasing in terms of pressure drop.

Bahiraei et al. [15] performed numerical solutions for the circular mini-channel through the finite volume method to examine the displacement of the particles in the nanofluid flows. They evaluated that their numerical solutions were in good agreement with correlation and experimental results. They determined that the locations of the particles are denser in the center and the density decreases in the regions close to the radius. They analyzed the particle displacement effect by comparing numerical solutions with the experimental Nusselt number and stated that the data are more optimistic with the experimental results if particle displacement is included. As an interesting result, they found that the generation of entropy by friction decreases as a result of increased particle size. Under the flow condition with larger particles, the

particles were evaluated to be more in the center and less in areas close to the pipe wall. They stated that this situation causes the viscosity to be lower in near-wall regions although the velocity gradient becomes higher. They explained the reason for entropy generation based on friction with this phenomenon.

Mahdavi et al [16] studied the nanofluids by performing two-phase numerical simulations in a vertical cylindrical tube. They compared Lagrangian and Eulerian approaches. They simulated each solid nanoparticle motion with the DPM model by force equilibrium equation. In the Eulerian approach, they emphasized that the results of the Mixture model are highly dependent on the correlations of the thermophysical properties of the mixture fluid and that it is less accurate than the DPM model. They showed this effect in velocity profiles by including the effect of slip velocity between the nanoparticle and base fluid with the DPM model approach. They repeated the analysis both in 2D and in 3D. When looking at the results, it was clear that the 2D approach only migrates particles in the radial direction, whereas in the 3D model, particles have movement in both radial and tangential directions. They concluded that the 3D approach is more reliable in comparison.

Hussein et al. [17] investigated the effect of nanofluids formed with SiO2 and TiO2 particles on thermal effectiveness in automobile radiators. While both nanofluids increase thermal performance, they observed that SiO2 has a higher thermal performance. They evaluated that the effectiveness enhancement for SiO2 was 32% while the effectiveness enhancement was around 29.5%.

Hussein et al. [18] carried out comparative experiments for pure water and nanofluid formed with SiO2 particles in industrial car radiators. They validated the experiments with the numerical model and stated that the results are in good agreement with the numerical model. They evaluated that heat transfer increases at increasing coolant flow rate and volumetric concentration, while friction factor decreases. They calculated that the rate of increase of the highest Nusselt number is approximately 56%.

Ali et al. [19] examined different coolant flow rates and airflow rates to create different heat loads in the cooling system of the Toyota Yaris car. They evaluated thermal characteristic behaviors for 4 different (0.1%–0.5%–1%–2%) concentration of Al2O3 in pure water at the cooling system. They stated that, with increasing concentration rates, there is a continuous increase in pumping power, while the rate of increase in heat transfer is not continuous. They evaluated that the optimum concentration rate is 1%. It was clear that thermal performance parameters deteriorate in the experiments conducted with the concentration ratios above 1%. They emphasized that the concentration ratio is an important point for thermal performance.

Mah et al. [20] analyzed analytically the situation in which there are laminar fully developed flow conditions for water-alumina fluid in the micro-channel by first and second law analysis. They stated that the flow is continuum due to the relatively small levels of Knudsen in analytical analysis, and it is reasonable to apply a no-slip boundary condition between the base fluid and the nanoparticle. They found that viscous dissipation increases with increasing nanoparticle amount and Reynolds number. They examined the changes in the Nusselt number with the increasing Reynolds number under fully developed flow conditions. They emphasized that there is no change in the Nusselt number when the viscous effects are neglected, whereas the Nusselt number is clearly reduced for the condition in which the viscous effects are included. They evaluated that the irreversibility caused by viscous dissipation can be neglected when compared to the irreversibility caused by flow friction.

Rashidi et al. [21] investigated the forced convection problem with nanofluids around a rotating cylinder using the finite volume method. They determined the rotation rate, Reynolds number, and nanoparticle volume fraction as variable parameters. They found that while there was a decrease in heat transfer with increasing rotation rate, heat transfer increased with the increasing amount of particles. Rashidi et al. [22] in a similar study investigated both the nanofluid behavior on a triangular obstacle and the magneto-hydrodynamic (MHD) effects on the flow. By adding the term external magnetic field to the momentum equations, they obtained results with the finite volume method. They found a decrease in Nusselt number with the increase of Stuart number, which defines magnetic effects.

Khan et al. [23–25] studied the MHD effects of nanomaterial flows in detail within the scope of entropy by developing their mathematical expressions with nonlinear partial differential equations using similarity variables. The Buongiorno nanofluid model was used in their mathematical modeling. In their work, they have provided a deep understanding of flow nature for engineers by including the terms mass and heat diffusion into their mathematical models.

Laein et al. [26] used PIV (Particle Image Velocimetry) to measure the laminar boundary layer thickness of TiO2 – water nanofluid on the vertical and horizontal plate at constant heat flux under natural convection conditions. They added 50–100 μm glass particles in order to track the velocity distribution in the fluid. They compared the experimental results with numerical analysis and theoretical analysis results. According to the results, they observed that adding nanoparticles to the base fluid (water) decreased the velocity boundary layer.

In addition to inserts such as baffles, twisted tape, vortex generators, nanofluids play an important role to improve heat transfer. Rashidi et al. [27] handled both nanofluids and inserts studies by making a comprehensive review study. Nanofluids, which are among quite wide applications, are also included in condensation and evaporation systems [28].

In the light of the above studies, the most important original part that distinguishes this study from other studies; the experimental setup for this study is to reach the fluid inlet temperature of 95 °C achieved in real automobile cooling systems and to compare the existing coolant (50:50 EG – water) with the new generation coolant (EG – Water – Al2O3) with a concentration of 0.5% at the different coolant flow rate and airflow rates. As a result of the study, it was determined that the use of nanofluid as a new generation coolant in the radiator increased the performance index by a maximum of 19.4%. While the entropy generation change increased on the coolant side, the opposite happened on the air side.

## 2. Nanofluid preparation

The authors examined the thermal properties of 3 different types (Al2O3, ZnO, and TiO2) nanoparticles in detail in their previous studies. They found that the nanoparticle with the best thermal behavior was Al2O3 and an increase of about 15.3% in heat transfer compared to the base fluid (water). Therefore, in the current study, experiments were carried out only with a mixture of Al2O3 nanoparticles. The nanoparticle properties of Al2O3 are given in Table 1 [29].

Nanofluid was prepared using the 2-step method. First, Al2O3 nanoparticles and 50–50% EG-Water base fluid were weighed with precision scales. (AND GX – 600, Max Mass:610 g, Deviation: 0.001 g). After Al2O3 nanoparticles were added in 50% EG – Water base fluid in a 600 mL glass beaker, it was placed in a temperature-controlled heat bath (Brand / Model: Cole Parmer / EW – 12108–25, Temperature: −20 to 200° C, Bath Capacity: 6 L, Heating Power: 1 kW, Cooling Power: 200 W, Flow: 11–24 L/min). Here, the mix-

**Table 1**
Nanoparticle properties.

| Nanoparticle | Al2O3 |
|---|---|
| Purity | 99.8% |
| Avg. Particle Diameter | 13 |
| Specific Surface Area (m2/g) | 85–115 |
| Shape | Nearly spherical |
| Density (kg/m3) | 3890 |
| Specific Heat (J/kgK) | 778 |
| Thermal Conductivity (J/kgK) | 45 |

ture was subjected to ultrasonic vibration with a probe-type homogenizer (Brand / Model: Optic Ivymen System / CY – 500, Power: 500 W, Frequency: 20 kHz, Probe Diameter / Length: Ø5, 6 / 60 mm). No surfactant was used. 8 L nanofluid was prepared for the test installation.

## 3. Experimental setup and calculations

### 3.1. Experimental setup

The experimental setup set up for thermal calculations is shown in Fig. 1. The experimental setup consists of a fluid tank, high-temperature centrifugal pump, automobile radiator, centrifugal fan, and an air duct that accelerates the air velocity to the radiator.

The prepared nanofluid is taken from the fluid tank with the help of a pump (Pentax, Ultra 3S–100–5, up to 80 lt/min) and is transferred to the radiator by passing through the flow meter (ABB, FEH311, 1–90 lt/min) with 0.4% reading accuracy. The flow rate of the fluid circulating in the system is adjusted by 2 valves at the pump outlet. The blower fan (Eurovent, EU 352, gives 3780 $m^3$/h at 981 Pa total pressure) used to cool the radiator is driven by a frequency converter (Siemens, Micro Master MM550-3, 5.5 kW) to reach different air velocities. In order to model the engine heat load, the fluid is heated with 2 thermal resistances of 3x2.5 kW (Total heat load: 15 kW, 220/380 V). A thermostat (Enda, ET5412) is used to keep the temperature of the fluid entering the radiator under constant conditions. NTC temperature sensor (Vishay, NTCLE300E3103SB, −40~+125 °C) with an accuracy of ±1.02 °C and pressure sensors (ITEC, P103, 0–1 bar) with an accuracy of 0.4% / 10 K (>20 °C) are placed to measure the temperature and pressure at the radiator inlet–outlet. K type thermocouples (Elimko, MI04–1 K30–10 – K20, K type) are used to measure the inlet–outlet air temperatures. The air-side velocity and pressure of the radiator are measured by the pitot tube (Testo, 350 M / XL-454, 0–200 mbar). Data logger (MC, IOTech Personal DAQ 3000) is used to record and read the measured temperature data.

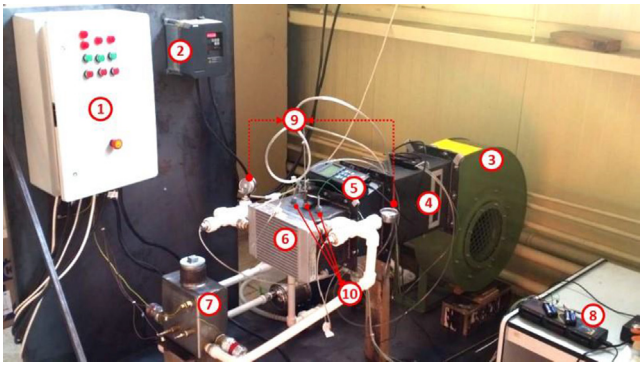


**Fig. 1.** Experimental setup; 1) control panel, 2) frequency converter, 3) fan, 4) duct, 5) velocity & pressure sensor, 6) radiator, 7) fluid tank, 8) data acquisition device, 9) barometers, and 10) static pressure – velocity – temperature measurement point.

In the experimental setup, a Peugeot automobile R4 type radiator made of aluminum material with louver fin type is used. The schematic view of the radiator geometry and basic radiator geometry information is given in Fig. 2.

### 3.2. Experimental procedure

In the experimental setup, heat transfer (Q), fan, and pump power ($P_f - P_p$), irreversibility ($I$) were investigated. In order to model the operating conditions, 2 different air velocities (4–5 m/s), and 3 different coolant flow rates (10–15 to 20 lt/min) were studied. The inlet coolant fluid temperature to the radiator was kept constant at 95 °C until it reached a steady-state regime in the heat bath. In order to adjust the air velocity to the desired value, the fan was first run at different frequencies. After obtaining the correlation equation between air velocity and frequency, the frequency of the desired air velocity was adjusted from the frequency converter. The valve at the radiator outlet was opened gradually and the pressure values in the system were followed. In the pressure gauge, it was seen that an active measurement was made after 25 lt/min. Therefore, pressure losses for 0–25 to 30–35 to 40–45 to 50–55 lt/min were measured and a curve was obtained for the pressure losses.

This curve was used in calculations for coolant flow rates below 25 lt/min. A manometer was used to measure the pressure loss on the air side of the radiator. The air leaving the radiator was released into the atmosphere.

### 3.3. Heat transfer analysis

Density and specific heat calculations, which are frequently used in thermal calculations, are given in Eqs. (1) and (2). While the ideal gas law is used in density calculations for the air side of the radiator, the specific heat is accepted as constant. Thermal properties are defined at the average temperature for the calculations [21].

$$\rho_{nf} = \rho_{nf}\phi - \rho_{bf}(1-\phi) \tag{1}$$

$$c_{nf} = \frac{\rho_{np}c_{np}\phi + \rho_{nf}c_{nf}(1-\phi)}{\rho_{nf}} \tag{2}$$

Heat capacity rate for air side is given by [7],

$$C_a = \dot{m}_a c_{p,a} = (\rho_a A_{cs,a} V_a) c_{p,a} \tag{3}$$

Heat capacity rate for coolant fluid (nanofluid) side is given by [7],

$$C_{nf} = \dot{m}_{nf} c_{p,nf} = (\rho_{nf} \dot{\forall}_{nf}) c_{p,nf} \tag{4}$$

Heat transfer leaving to the air side is given by [7],

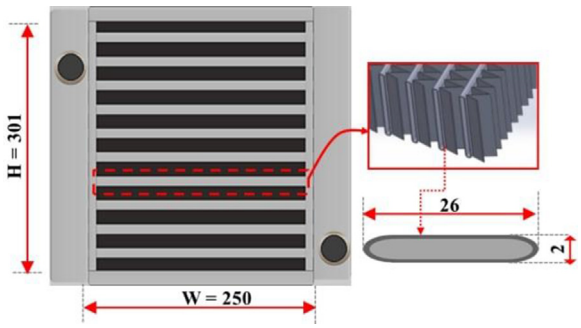


**Fig. 2.** Radiator schematic view and geometry information (Unit: mm).

$$Q_{nf} = \dot{m}_{nf} c_{p,nf} (T_{nf,i} - T_{nf,e}) \quad (5)$$

Maximum heat transfer expected to be released to the air side is given by [7],

$$Q_{max} = C_{min} (T_{nf,i} - T_{a,i}) \quad (6)$$

where $C_{min}$ belongs to the air side and $C_{min} = C_a$, $C_{max} = C_{nf}$. For cross – flow unmixed fluid, the effectiveness value is given in Eq. (7) according to the NTU (Number of Transfer Unit) method [7],

$$\varepsilon = 1 - \exp\left\{ \left( NTU^{0.22} / C^* \right) \left[ \exp\left( -C^* NTU^{0.78} \right) - 1 \right] \right\} \quad (7)$$

where $C^*$ expression indicates the capacity ratio and is calculated by Eq. (8) [7],

$$C^* = Cmin/Cmax \quad (8)$$

Now, pressure losses calculations for the coolant side are calculated according to the curve fitting equation in Fig. 3. Then, the pump power can be calculated with Eq. (9) [7],

$$P_p = \dot{\forall}_{nf} \Delta P_{nf} / \eta_p \quad (9)$$

Air side pressure loss measurement is calculated with a manometric pressure device connected from the radiator inlet and outlet. Pressure loss due to friction along the short channel is neglected. Fan power has been calculated by [7],

$$P_f = (HW)_{cs} V_a \Delta P_a / \eta_f \quad (10)$$

where H and W are the core height and width dimensions of the radiator, and $V_a$ is the air velocity value measured from the front surface of the radiator. Radiator dimensions required for thermal calculations are shown in Table 2.

Now, the performance index ($PI$) of the radiator can be calculated by [7],

$$PI = Q_{nf} / (P_f + P_p) \quad (11)$$

The other method to evaluate radiator performance has been entropy based studies. Coolant side is incompressible liquid, and air side is accepted as ideal gas compressible. In that case, entropy generation can be defined as [7];

$$S_{gen} = S_{gen,a} + S_{gen,nf} \quad (12)$$

where $S_{gen,a}$ and $S_{gen,nf}$ expressions indicate the entropy generation at the air side and coolant side are calculated by Eq. (13) and Eq. (14) [7],

$$S_{gen,a} = \dot{m}_a \left[ c_{p,a} ln\left( \frac{T_{a,e}}{T_{a,i}} \right) - R_a ln\left( \frac{P_{a,e}}{P_{a,i}} \right) \right] \quad (13)$$

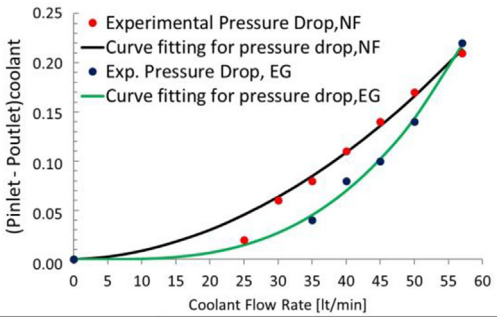


| | |
|---|---|
| (Pinlet - Poutlet)coolant, EG+Water | = 0.00006003$\dot{\forall}^2$ + 0.00033166$\dot{\forall}$ - 0.00024893 |
| (Pinlet - Poutlet)coolant, Al2O3+EG+Water | = 0.00000140$\dot{\forall}^3$ – 0.00001350$\dot{\forall}^2$ + 0.00005048$\dot{\forall}$ - 0.00001907 |

**Fig. 3.** Pressure drop for coolant side.

**Table 2**
Radiator core and fin geometry.

| | |
|---|---|
| Core Width × Height × Depth (WxHxD) | 250 × 301 × 60.4 |
| Tube outer dimensions | 2 × 26 mm |
| Tube thickness | 0.5 mm |
| Tube inner dimensions | 1 × 25 mm |
| Tube hydraulic diameter | 1.923 mm |
| Number of Tubes | 34 |
| Fin pitch (fin/inch) | 20 fpi |
| Fin type | Louver |
| Fin material | Aluminum |

$$S_{gen,nf} = \dot{m}_{nf} \left[ c_{p,nf} ln\left( \frac{T_{nf,e}}{T_{nf,i}} \right) - \frac{P_{nf,e} - P_{nf,i}}{\rho_{nf} T_{nf,avg.}} \right] \quad (14)$$

It should be noted that the entropy generation of the coolant side is a negative value and air side is a positive value. For heat exchangers, the total irreversibility that occurs on both the coolant and the air side can be calculated by entropy generation. Total irreversibility is given in Eq. (15) [7],

$$I = T_0 S_{gen} \quad (15)$$

Besides, inlet–outlet temperatures for air and coolant sides are measured. With the help of the NTU method, comparisons of NTU, capacity ratio, and effectiveness values of heat exchanger have been calculated.

## 4. Uncertainty analysis

Uncertainty analysis calculations can be divided into two parts: a) the uncertainty of a directly measured variable, and b) the uncertainty of an indirectly measured variable.

Experimental uncertainties were determined using the method proposed by Kline and McClintock [30]. The data obtained are given in Appendix 1 and 2. According to the calculations, the maximum uncertainty in heat transfer was found to be 26.25% and 12.73% for speed and pressure drop, respectively.

## 5. Results and discussion

In this study, the effect of nanofluid use in industrial automobile radiators on thermal characteristics was investigated experimentally. The effect of engine operating conditions on radiator thermal performance is very important. Especially after a certain period of time, the inlet coolant fluid temperature reaches high-temperature levels such as 90–100 °C [31]. Therefore, the coolant inlet temperature was kept at 95° in the present study. A high NTU value in a heat exchanger means that the size of the heat exchanger also increases. Another way to increase the heat amount transferred would be to increase the total heat transfer coefficient. As a result of the experiments, it was determined that the NTU value in Table 3 increased with the use of nanofluid. The maximum increase in NTU value was 16.4% at 4 m/s air velocity and 10C.F.R. We can say that a performance increase of 16.4% occurs with the use of nanofluid by keeping the radiator size constant. In response to this performance increase, a heat exchanger with a 16.4% reduced area surface means that it will provide the same cooling load using nanofluid. This increase in thermal conductivity can be thought to be due to Brownian motion, clustering, and solid/liquid interface interactions of the particles. Keblinski et al. [32] said that Brownian motion is too slow to transfer heat through nanofluid. However, they mentioned that this movement indirectly increases the heat conduction by causing the clustering of particles. The interface effect that can increase thermal conduction is known as the layering of the liquid on the solid surface. Liquid layering at the interface is expected to

**Table 3**
Effectiveness, NTU, Heat transfer and Irreversibility results.

| Mixture type | EG – Water | | | EG – Water – Al2O3 | | | EG – Water | | | EG – Water – Al2O3 | | |
|---|---|---|---|---|---|---|---|---|---|---|---|---|
| Air velocity | 4 m/s | | | | | | 5 m/s | | | | | |
| C.F.R., lt/min | 10 | 15 | 20 | 10 | 15 | 20 | 10 | 15 | 20 | 10 | 15 | 20 |
| $C_a = C_{min}$ | 0.425 | 0.419 | 0.414 | 0.422 | 0.423 | 0.419 | 0.534 | 0.534 | 0.536 | 0.536 | 0.531 | 0.531 |
| $C_{nf} = C_{max}$ | 0.619 | 0.930 | 1.240 | 0.619 | 0.935 | 1.239 | 0.619 | 0.930 | 1.240 | 0.625 | 0.929 | 1.245 |
| $C^* = C_{min}/C_{max}$ | 0.685 | 0.451 | 0.334 | 0.682 | 0.453 | 0.338 | 0.861 | 0.575 | 0.432 | 0.858 | 0.572 | 0.427 |
| $\varepsilon = Q/Q_{max}$ | 0.357 | 0.392 | 0.410 | 0.395 | 0.417 | 0.425 | 0.327 | 0.346 | 0.361 | 0.348 | 0.365 | 0.370 |
| *NTU* | 0.542 | 0.573 | 0.588 | 0.631 | 0.629 | 0.620 | 0.504 | 0.499 | 0.507 | 0.553 | 0.539 | 0.524 |
| Q(kW) | 10.72 | 11.68 | 12.04 | 11.74 | 12.14 | 12.09 | 12.23 | 13.09 | 13.67 | 13.03 | 13.26 | 13.27 |
| *Q (Change of %)* | * | * | * | +9.5% | +3.9% | +0.4% | * | * | * | +6.5% | +1.3% | −2.9% |
| *I (W)* | 2893.71 | 2597.62 | 2984.71 | 930.71 | 1303.21 | 1618.51 | 3456.07 | 4056.07 | 4253.19 | 1728.52 | 2200.73 | 2617.01 |
| *I (Change of %)* | * | * | * | −67.8% | −49.8% | −45.7% | * | * | * | −49.9% | −45.7% | −38.4% |

*The changes were calculated according to base fluid (50:50 EG + water).

provide much higher thermal conduction. As can be seen in Fig. 4 (a), the temperature of the coolant fluid leaving the radiator has increased with the increasing coolant flow rate. However, heat transfer has increased due to the high amount of fluid passing per unit time. Compared to the EG-Water mixture, the use of nanofluid increased heat transfer by a maximum of 9.5% for 4 m/s air velocity and 10 lt/min coolant flow rate. There was no change in the pressure drop on the coolant side with the increase of the flow velocity on the air side of the radiator. However, as the increased air velocity increased the amount of heat transfer, the temperature of the air leaving the radiator increased. It is clearly seen in Fig. 4 (b) that the use of nanofluid increases the radiator air outlet temperature. An increase in pressure loss was observed on the coolant side due to the nanoparticle structures which increase the viscosity of the mixture.

The pressure increase on the coolant side seems to be a disadvantage as it causes an increase in pump power consumption. However, it is necessary to compare this disadvantage with the improvement in heat transfer. The performance index of heat exchangers provides important information on this subject. Performance index values calculated with Eq. (11) are shown in Fig. 5(a). When the extra consumption of pump power and the heat transfer enhancement are compared, the use of nanofluid shows an improvement compared to the EG-Water mixture. Performance index increase was realized by 19.4% at 4 m / s air velocity and 10 CFR. It has been observed that the increase in air velocity decreases the performance index because the increase in fan power consumption dominates the increase in heat transfer enhancement. With the increasing coolant flow rate, the effectiveness of the radiator has increased in all cases. The use of nanofluid has increased the effectiveness maximum of approximately 10.4% at 4 m/s air velocity and 10 lt/min C.F.R (Coolant Flow Rate).

In order to evaluate the radiator performance through the second law, irreversibilities occurring both inside the radiator and on the air side were calculated with experimental data. As can be seen from Fig. 6(a), the change in entropy generation on the coolant side has negative values due to the heat loss caused by the temperature difference. Comparing EG-water and NF in terms of entropy generation change on the coolant side, the use of nanofluid occurred more entropy change with a 9.7% difference for 4 m / s air velocity and 10C.F.R. However, for entropy generation change of the air side, nanofluid usage occurred less entropy change with a 9.5% difference. However, with increasing coolant flow rate, entropy generation decreases on the coolant side, while the opposite increases on the air side. The major role of entropy generation in the radiator is the irreversibility caused by the temperature difference. It is understood in Fig. 6(b) that the entropy generation caused by the pressure drop is negligible compared to the entropy generation due to the temperature difference. Important decreases in total irreversibility were observed when using nanofluid compared to the EG-Water mixture.

Maximum irreversibility occurred in EG – Water mixture at 5 m/s air velocity – 20 lt/min C.F.R. It is understood from the irreversibility results given in Fig. 7 that entropy generation is in an increasing trend with the increase of both air velocity and coolant flow rate. When nanofluid.

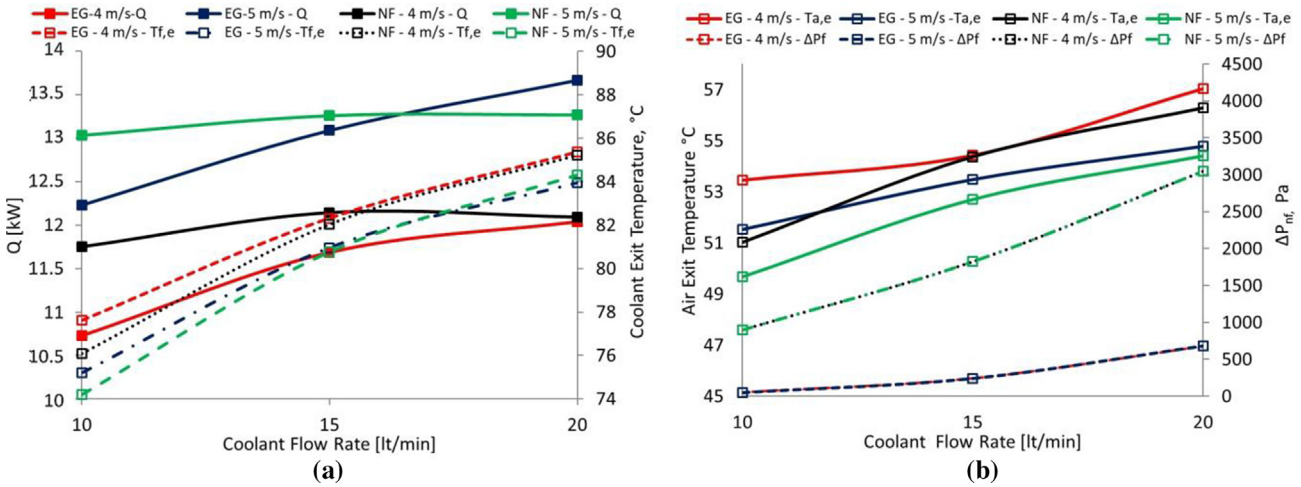


**Fig. 4.** (a) Heat transfer and coolant exit temperature with coolant flow rate, (b) coolant side pressure drop and air exit temperature with coolant flow rate.

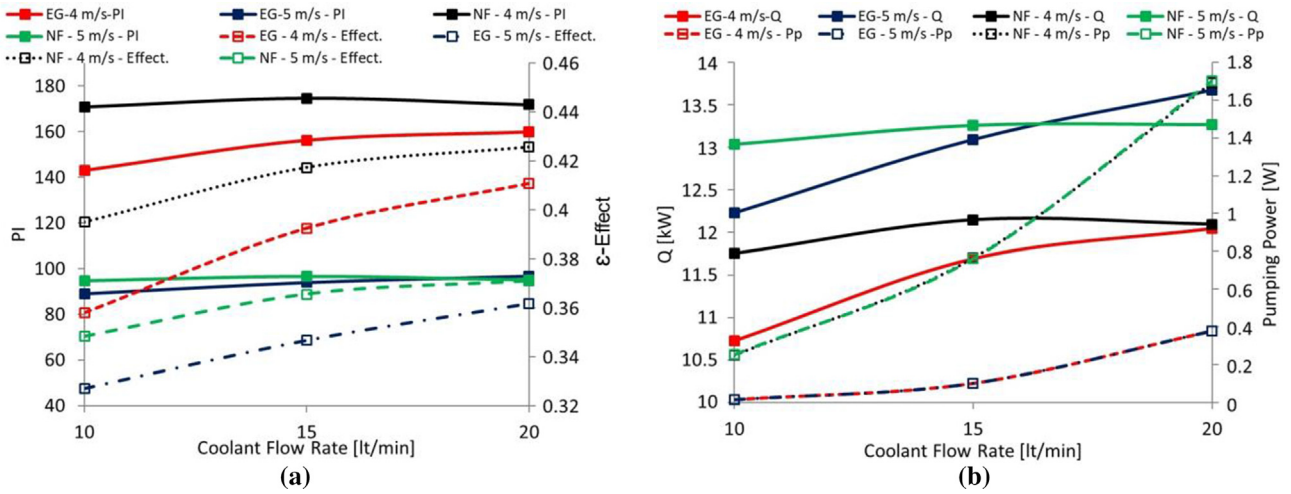


**Fig. 5.** (a) Performance index and effectiveness with coolant flow rate, (b) heat transfer and pumping power with coolant flow rate.

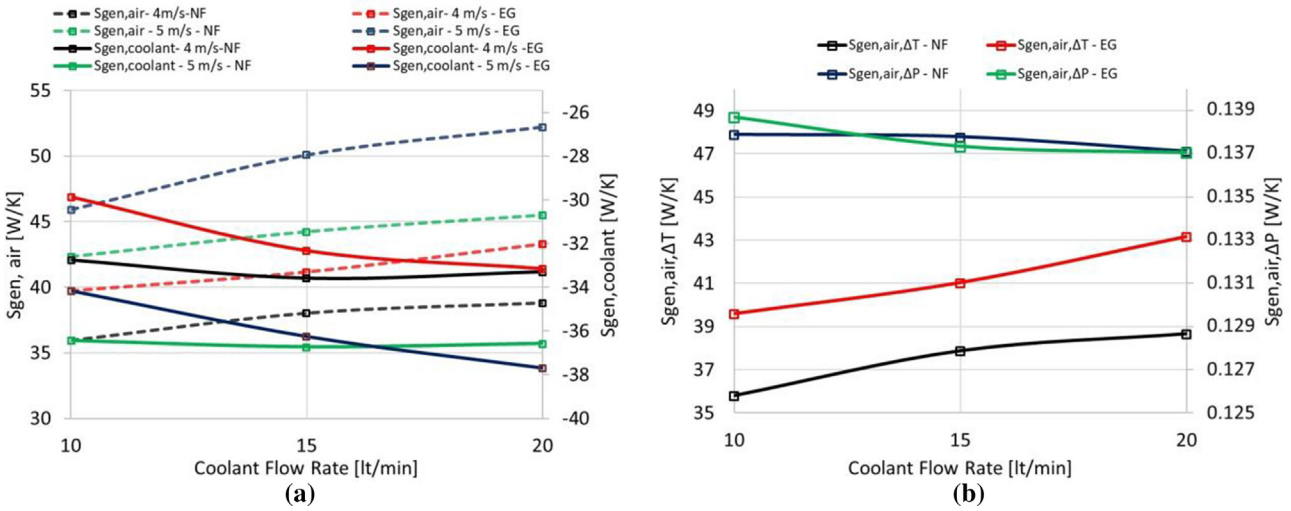


**Fig. 6.** (a) Air and coolant side entropy gen. with coolant flow rate, (b) entropy generation due to temperature difference and pressure drop at the air side for air velocity = 4 m/s.

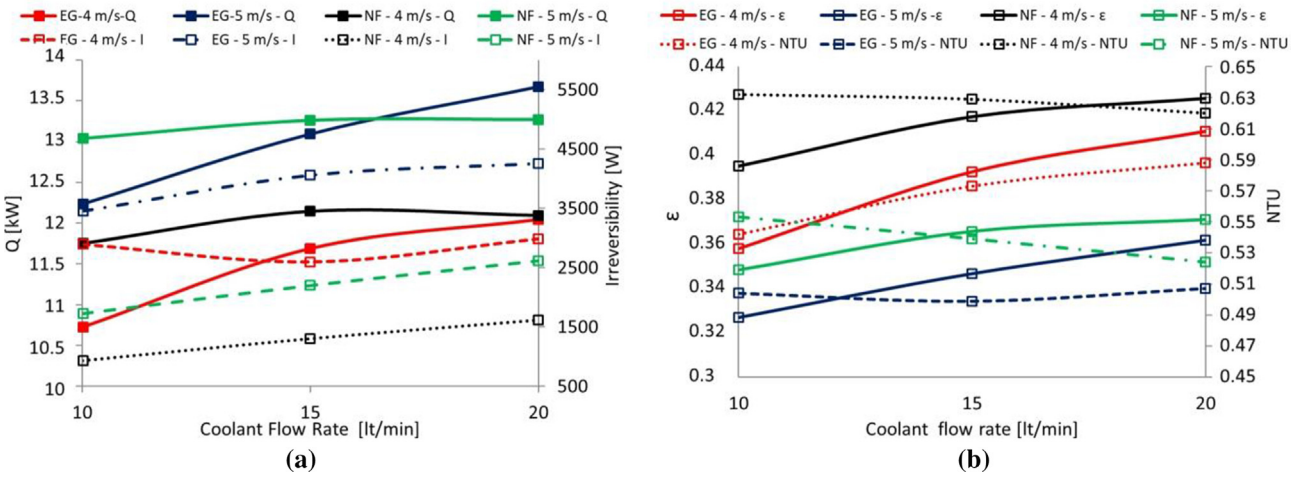


**Fig. 7.** (a) Heat transfer and irreversibility with coolant flow rate, (b) effectiveness and NTU values with coolant flow rate.

was used, approximately 68% reduction in terms of irreversibility occurred at the 4 m / s air velocity and 10 lt / min C.F.R. compared to conventional case. Table 3 contains the results of the use of nanofluid and its effects on both heat transfer and irreversibility.

## 6. Conclusions

In this study, the working conditions were experimentally experienced on two different mixing fluids formed with EG – Water and EG – Water – Al2O3 at the louver blade type Peugeot R4 automobile radiator. In order to model the real working conditions of automobile radiators, the coolant fluid's high inlet temperature constitutes an important part of this study. Energy, entropy, and irreversibility calculations were made with the data obtained from the experiments. The results obtained throughout the study are as follows;

- The nanofluid used in automobile radiators has shown significant improvements in heat transfer compared to EG-Water. The maximum heat transfer increase with 9.5% occurred at 4 m/s air velocity and 10 lt/min coolant flow rate. Also, the best effectiveness of the radiator occurred at an air velocity of 4 m/s.
- A general disadvantage of using nanofluid is the increase in pump power. However, the performance index was evaluated to compare it with the heat transfer enhancement achieved. The maximum performance index increase with the use of nanofluid was approximately 18.8% for 4 m / s air velocity and 10 CFR.
- In entropy calculations, the entropy change on the coolant side was negative values due to heat loss, while the entropy change on the air side was positive values. With increasing coolant flow rate, entropy generation increased on the air side, while a decrease occurred on the coolant side. While the maximum entropy generation in the base (50:50 EG – Water) case was 14.51 W/K at 5 m / s air velocity and 20 CFR, it was approximately 8.93 W/K under the same operating conditions with the new generation cooling.
- It has been observed that the entropy generated by the temperature difference is considerably higher than the entropy value generated due to the pressure loss, so the entropy generated due to the pressure loss is negligible.
- The highest irreversibility occurred at 5 m/s air velocity and 20 lt/min coolant flow rate with EG – Water mixture. High air velocity and high coolant flow rate have increased the amount of irreversibility.

Large-sized radiators are produced in order to provide the heat loads caused by increasing automobile performances. Therefore, the use of nanofluids in automobile radiators is a good option for heat transfer enhancement, which is still under investigation and will continue to be explored.

## Declaration of Competing Interest

The authors declare that they have no known competing financial interests or personal relationships that could have appeared to influence the work reported in this paper.

## Acknowledgments

This project was supported by "The Scientific and Technological Research Council of Turkey" (TUBITAK 1505, Project Number 5140013) and Kale Oto Radyatör Sanayi ve Ticaret A.Ş. The authors gratefully acknowledge the financial supports provided by TUBITAK and Kale Oto Radyatör.

**Appendix 1. Uncertainties of variables measured.**

| No. | Instrument | Range of instrument | Variable measured | Total uncertainty | Values measured in experiment | | | Uncertainty | |
|---|---|---|---|---|---|---|---|---|---|
| | | | | | Min | Max | | Min | Max |
| 1 | NTC Temperature Sensor (Vishay, NTCLE300E3103SB) | −40 to 125 °C | Fluid inlet temperature,$T_i$ | $U_{Fixed,T_i} = \pm 1.02°C$<br>$U_{Random,T_i} = \pm t\sigma/\sqrt{n}(\%90) = 0°C$<br>$U_{T_i} = \sqrt{U^2_{Fixed,T_i} + U^2_{Random,T_i}}$<br>$= \sqrt{1.02^2 + 0^2} \cong \pm 1.02°C$ | $T_i$(°C) | | | $U_{T_i}/T_i$ | |
| | | | | | 94.8 | 95.1 | | 1.0726% | 1.0759% |
| 2 | NTC Temperature Sensor (Vishay, NTCLE300E3103SB) | −40 to 125 °C | Fluid exit temperature,$T_e$ | $U_{T_e} = \sqrt{1.02^2 + 0^2} \cong \pm 1.02°C$ | $T_e$(°C) | | | $U_{T_e}/T_e$ | |
| | | | | | 74.2 | 89.6 | | 1.1384% | 1.3747% |
| 3 | Pressure transmitter (ITEC, P103) | 0 ~ 1 bar | Pressure drop,$\Delta P$ | $U_{\Delta P} = 1 \times \frac{0.4\%}{10K} \times (90 - 20) \cong \pm 0.028bar$ (from specifications) | $\Delta P(bar)$ | | | $U_{\Delta P}/\Delta P$ | |
| | | | | | 0 | 0.22 | | 12.727% | – |
| 4 | Flow meter (ABB, FEH311,) | 1 ~ 90 lt/min | Volume flow rate,$\dot{\forall}$ | $U_{\dot{\forall}} = \sqrt{0.1^2 + 0^2} \cong \pm 0.1lt/min$ | $\dot{\forall}(lt/min)$ | | | $U_{\dot{\forall}}/\dot{\forall}$ | |
| | | | | | 10.0 | 25.0 | | 0.04% | 1.0% |
| 5 | Thermophysical properties (Equation) | – | Density, $\rho$ Specific heat,$c_p$ | $U_\rho/\rho = \sqrt{(0)^2 + (0)^2 + (0.03\%)^2} = \pm 0.03\%$ $U_{c_p}/c_p = \sqrt{(0)^2 + (0)^2 + (0.10\%)^2} = \pm 0.1\%$ | | | | | |

**Appendix 2. Uncertainty of results calculated..**

| No | Result | Maximum uncertainty |
|---|---|---|
| 1 | Mass flow rate,$\dot{m} = \rho\dot{\forall}$ | $\frac{U_{\dot{m}}}{\dot{m}} = \left[\left(\frac{\partial\dot{m}}{\partial\rho}\cdot\frac{U_\rho}{\dot{m}}\right)^2 + \left(\frac{\partial\dot{m}}{\partial\dot{\forall}}\cdot\frac{U_{\dot{\forall}}}{\dot{m}}\right)^2\right]^{0.5} = \left[(0.03\%)^2 + (1.0\%)^2\right]^{0.5} = 1.00\%$ |
| 2 | Temperature difference of fluid from inlet to exit,$\Delta T = T_e - T_i$ | $\frac{U_{\Delta T}}{\Delta T} = \left[\left(\frac{\partial\Delta T}{\partial T_e}\cdot\frac{U_{T_e}}{\Delta T}\right)^2 + \left(\frac{\partial\Delta T}{\partial T_i}\cdot\frac{U_{T_i}}{\Delta T}\right)^2\right]^{0.5} = \left[\left(\frac{1.02}{5.5}\right)^2 + \left(\frac{1.02}{5.5}\right)^2\right]^{0.5} = 26.23\%$ |
| 3 | Heat transfer,$\dot{Q} = \dot{m}c_p\Delta T$ | $\frac{U_{\dot{Q}}}{\dot{Q}} = \left[\left(\frac{\partial\dot{Q}}{\partial\dot{m}}\cdot\frac{U_{\dot{m}}}{\dot{Q}}\right)^2 + \left(\frac{\partial\dot{Q}}{\partial c_p}\cdot\frac{U_{c_p}}{\dot{Q}}\right)^2 + \left(\frac{\partial\dot{Q}}{\partial\Delta T}\cdot\frac{U_{\Delta T}}{\dot{Q}}\right)^2\right]^{0.5} = \left[(1.0\%)^2 + (0.1\%)^2 + (26.23\%)^2\right]^{0.5} = 26.25\%$ |

## References


[1] İ. Atmaca, S.K. Soylu, M. Asiltürk, A. Doğan, Improving heat transfer performance of an automobile radiator using Cu and Ag doped TiO2 based nanofluids, Appl. Therm. Eng. 157 (2019) 1–9.

[2] S. Patel, S.P. Deshmukh, Analytical design and verification of automotive radiator using 1-D simulation, Int. J. Res. Appl. Sci. Eng. Technol. (2017) 2349–2360. ISSN:2321-9653.

[3] S.S. Chougule, S.K. Sahu, Comparative study of cooling performance of automobile radiator using Al2O3-water and carbon nanotube-water nanofluid, J. Nanotechnol. Eng. Med., 5 (1), 010901-1–010901-6, 2014.

[4] S.M. Peyghambarzadeh, S.H. Hashemabadi, S.M. Hoseini, M.S. Jamnani, Experimental study of heat transfer enhancement using water/ethylene glycol based nanofluids as a new coolant for car radiators, Int. Commun. Heat Mass Transf. 38 (9) (2011) 1283–1290.

[5] C. Qi, N. Zhao, J. Tang, X. Cui, Experimental study on influences of cylindrical grooves on thermal efficiency, exergy efficiency and entropy generation of CPU cooled by nanofluids, Int. J. Heat Mass Transf. 135 (2019) 16–32.

[6] A. Ahmed, H. Baig, S. Sundaram, T.K. Mallick, Use of nanofluids in solar PV/thermal systems, Int. J. Photoenergy 1–17 (2019).

[7] R.R. Sahoo, P. Ghosh, J. Sarkar, Energy and exergy comparisons of water based optimum brines as coolants for rectangular fin automotive radiator, Int. J. Heat Mass Transf. 105 (2017) 690–696.

[8] C. Selvam, R.S. Raja, D.M. Lal, S. Harish, Overall heat transfer coefficient improvement of an automobile radiator with graphene based suspensions, Int. J. Heat Mass Transf. 115 (2017) 580–588.

[9] E.M.C. Contreras, G.A. Oliveira, E.P.B. Filho, Experimental analysis of the thermohydraulic performance of graphene and silver nanofluids in automotive cooling systems, Int. J. Heat Mass Transf. 132 (2019) 375–387.

[10] M. Gollin, D. Bjork, Comparative Performance of Ethylene Glycol/Water and Propylene Glycol/Water Coolants in Automobile Radiators, SAE Technical Paper 960372, 1996.

[11] P. Chaurasia, A. Kumar, A. Yadav, P.K. Rai, V. Kumar, L. Prasad, Heat transfer augmentation in automobile radiator using Al2O3 – water based nanofluid, SN Appl. Sci. (2019) 1–7.

[12] G. Liang, I. Mudawar, Review of single-phase and two-phase nanofluid heat transfer in macro-channels and micro-channels, Int. J. Heat Mass Transf. 136 (2019) 324–354.

[13] G. Huminic, A. Huminic, The heat transfer performances and entropy generation analysis of hybrid nanofluids in a flattened tube, Int. J. Heat Mass Transf. 119 (2018) 813–827.

[14] N. Zhao, J. Yang, H. Li, Z. Zhang, S. Li, Numerical investigations of laminar heat transfer and flow performance of Al2O3–water nanofluids in a flat tube, Int. J. Heat Mass Transf. 92 (2016) 268–282.

[15] M. Bahiraei, C. Kazerooni, Second law analysis of nanofluid flow within a circular minichannel considering nanoparticle migration, Entropy 1–27 (2016).

[16] M. Mahdavi, M. Sharifpur, J.P. Meyer, CFD modelling of heat transfer and pressure drops for nanofluids through vertical tubes in laminar flow by Lagrangian and Eulerian approaches, Int. J. Heat Mass Transf. 88 (2015) 803–813.

[17] A.M. Hussein, R.A. Bakar, K. Kadirgama, K.V. Sharma, Heat transfer augmentation of a car radiator using nanofluids, Heat Mass Transf. 1–9 (2014).

[18] A.M. Hussein, R.A. Bakar, K. Kadirgama, Study of forced convection nanofluid heat transfer in the automotive cooling system, Case Stud. Thermal Eng. 2 (2014) 50–61.

[19] M. Ali, M. El-Leathy, Z.A. Sofyany, The effect of nanofluid concentration on the cooling system of vehicles radiator, Adv. Mech. Eng. 1–13 (2014).

[20] W.H. Mah, Y.M. Hung, N. Guo, Entropy generation of viscous dissipative nanofluid flow in microchannels, Int. J. Heat Mass Transf. 55 (2012) 4169–4182.

[21] S.Z. Shirejini, S. Rashidi, J.A. Esfahani, Recovery of drop in heat transfer rate for a rotating system by nanofluids, J. Mol. Liq. 220 (2016) 961–969.

[22] S. Rashidi, M. Bovand, J.A. Esfahani, Opposition of magnetohydrodynamic and AL2O3–water nanofluid flow around a vertex facing triangular obstacle, J. Mol. Liq. 215 (2016) 276–284.

[23] J. Wang, M. Riaz Muhammad, W.A. Ijaz Khan, S.Z. Abbas, Entropy optimized MHD nanomaterial flow subject to variable thicked surface, Comput. Methods Programs Biomed. 189 (2020) 1–7.

[24] S.Z. Abbas, M. Ijaz Khan, S. Kadry, W.A. Khan, M. Israr-Ur-Rehman, M. Waqas, Fully developed entropy optimized second order velocity slip MHD nanofluid flow with activation energy, Comput. Methods Programs Biomed. 190 (2020) 1–7.

[25] Riaz Muhammad, M. Ijaz Khan, Niaz B. Khan, and Mohammed Jameel, Magnetohydrodynamics (MHD) radiated nanomaterial viscous material flow by a curved surface with second order slip and entropy generation, 189, 1-6, 2020.

[26] R. Parizad Laein, S. Rashidi, J. Abolfazli Esfahani, Experimental investigation of nanofluid free convection over the vertical and horizontal flat plates with uniform heat flux by PIV, Adv. Powder Technol. 27 (2016) 312–322.

[27] S. Rashidi, M. Eskandarian, O. Mahian, S. Poncet, Combination of nanofluid and inserts for heat transfer enhancement, J. Therm. Anal. Calorim. 135 (2019) 437–460.

[28] Saman Rashidi, Omid Mahian, Ehsan Mohseni Languri, Applications of nanofluids in condensing and evaporating systems, J. Therm. Anal. Calorim. 131 (2018) 2027–2039.

[29] A. Topuz, T. Engin, A.A. Özalp, B. Erdoğan, S. Mert, A. Yeter, Experimental investigation of optimum thermal performance and pressure drop of water-based Al2O3, TiO2 and ZnO nanofluids flowing inside a circular microchannel, J. Therm. Anal. Calorim. 131 (2018) 2843–2863.
[30] J.P. Holman, Experimental Methods for Engineers, 8th ed., McGraw-Hill, NewYork, 2012.
[31] D.R. Burke, A.J. Lewis, S. Akehurst, C.J. Brace, I. Pegg, R. Stark, Systems optimisation of an active thermal management system during engine warm-up, Proc. Instit. Mech. Eng., Part D 1–15 (2012) 2012.
[32] P. Keblinski, S.R. Phillpot, S.U.S. Choi, J.A. Eastman, Mechanisms of heat flow in suspensions of nano-sized particles (nanofluids), Int. J. Heat Mass Transf. 45 (2002) 855–863.